

Quantum Physics Letters
An International Journal

http://dx.doi.org/10.18576/qpl/080201

A Microscopic Analysis of Elastic Scattering Data for Eight Different Density Distributions of ¹⁵N Nucleus by ⁷Li, ⁹Be, ¹⁰B, ¹¹B, ¹²C, ¹³C and ²⁷Al Targets at Different Incident Energies

M. Aygun*

Department of Physics, Bitlis Eren University, Bitlis, Turkey

Received: 2 May 2019, Revised: 23 Jul. 2019, Accepted: 28 Jul. 2019

Published online: 1 Aug. 2019

Abstract: We examine the elastic scattering cross sections of ¹⁵N projectile on ⁷Li, ⁹Be, ¹⁰B, ¹¹B, ¹²C, ¹³C and ²⁷Al targets. The real part of the optical model potential is obtained for eight different density distributions of the ¹⁵N nucleus by using the double folding model with the M3Y interaction. The imaginary part of the optical potential is evaluated as the phenomenological Woods-Saxon potential. A good agreement between theoretical results and experimental data is achieved. Finally, new and practical analytical expressions for imaginary potential depths of each density examined with this study are given, for the first time. These equations will be useable in the calculations of the nuclear interactions with the ¹⁵N nucleus.

Keywords: Optical model, double folding model, elastic scattering

1 Introduction

The ¹⁵N nucleus is one of sixteen isotopes of nitrogen. It has 1/2 spin and negative parity. The ¹⁴N and ¹⁵N nuclei are rare stable isotopes of nitrogen [1]. ¹⁵N has low thermal neutron capture cross sections [1]. Also, the ¹⁵N nucleus is applied to nuclear magnetic resonance spectroscopy (NMR) owing to a fractional spin [2]. Therefore, the analysis of ¹⁵N nucleus reactions is still an important subject in the field of nuclear physics.

Nuclear reactions are a significant tool in understanding the nuclear structure. Elastic scattering is extensively used for this purpose. The elastic scattering studies of 15 N nucleus by different target nuclei can be found from the literature. In this respect, Rudchik et al. [3,4] measured the elastic scattering of 15 N from 7 Li and 9 Be at incident energies of 81 and 84 MeV, respectively. These data are analyzed with the coupled reaction channels (CRC) method. Burtebayev et al. [5] measured the elastic scattering experimental data of 15 N + 10,11 B reactions at E_{lab} =43 MeV. They applied the optical and the double folding models in order to explain the experimental data theoretically. Rudchik et al. [6]

achieved the experimental data of the elastic scattering of $^{15}\rm{N}$ + $^{12}\rm{C}$ reaction at $E_{\rm lab}$ =81 MeV. Gamp et al. [7] reported the elastic scattering data of $^{15}\rm{N}$ + $^{13}\rm{C}$ reaction at $E_{\rm lab}$ =30, 32 and 45 MeV. Prosser et al. [8] presented the elastic data of $^{15}\rm{N}$ + $^{27}\rm{Al}$ reaction at $E_{\rm c.m.}$ =21.1, 30.8, 39.9 and 44.9 MeV. They analyzed the experimental data for the fixed depths of real and imaginary potentials and variable values of the potentials by using the optical model

The density distribution is necessary in defining both structural and nuclear interactions of nuclei. Therefore, there has always been a quest for different density distributions that describe nuclei in a good way [9, 10, 11, 12, 13]. There are several known density distributions of the ¹⁵N nucleus. However, proposing new density distributions will be important in defining the ¹⁵N nucleus interactions.

The potential parameters are important inputs in the theoretical calculations of elastic scattering, inelastic scattering and transfer reactions. It is desirable to know these parameters when performing such calculations. In this context, when we examine ¹⁵N reactions over a wide

^{*} Corresponding author e-mail: murata.25@gmail.com



range of target nuclei, such a study is so far missing in the literature

In the present study, we analyze the elastic scattering angular distributions of ¹⁵N projectile by ⁷Li, ⁹Be, ¹⁰B, ¹¹B, ¹²C, ¹³C and ²⁷Al target nuclei at various incident energies. To produce the real part of the optical model potential, we use eight different density distributions of ¹⁵N. We calculate the elastic cross sections and compare the theoretical results with the experimental data. Then, we obtain the values of the optical potential parameters. With these potential parameters, we obtain new global sets of the imaginary potential.

The next section shows information on the calculation procedure. Section 3 presents the parametrization of the density distributions evaluated in our work. Section 4 gives the results and discussions. Finally, section 5 provides the conclusions.

2 Double Folding Model

The theoretical analysis of ¹⁵N elastic scattering by various targets is performed under the optical model. With this goal, the real part of the optical model potential is obtained with the help of the double folding model written as

$$V(\overrightarrow{r}) = \int d\overrightarrow{r}_1 \int d\overrightarrow{r}_2 \rho_P(\overrightarrow{r}_1) \rho_T(\overrightarrow{r}_2) \nu_{NN}(\overrightarrow{r} - \overrightarrow{r}_1 + \overrightarrow{r}_2),$$
(1)

where $\rho_P(\overrightarrow{r}_1)$ and $\rho_T(\overrightarrow{r}_2)$ are the densities of projectile and target, respectively. The effective nucleon-nucleon interaction potential v_{NN} is accepted as the M3Y (Michigan 3 Yukawa) nucleon-nucleon shown by [14]

$$v_{NN}(r) = 7999 \frac{\exp(-4r)}{4r} - 2134 \frac{\exp(-2.5r)}{2.5r} + 276 \left(1 - 0.005 \frac{E_{\text{Lab}}}{A_p}\right) \delta(r) \text{ MeV}.$$
(2)

The imaginary part of the optical model potential is assumed in the Woods-Saxon form

$$W(r) = -\frac{W_0}{1 + \exp\left(\frac{r - R_w}{a_w}\right)}, \quad R_w = r_w \left(A_P^{1/3} + A_T^{1/3}\right)$$
(3)

where W_0 , r_w , and a_w are the depth, radius and diffuseness parameters of the imaginary potential, respectively. Also, A_P and A_T are the mass numbers of projectile and target, respectively. The code FRESCO [15] is used in the calculations.

3 Parametrization of density distributions of projectile and target nuclei

3.1 Density distributions of ¹⁵N projectile

3.1.1 Ngô - Ngô density distribution

The Ngô - Ngô density distribution is shown by [16, 17]

$$\rho_i(r) = \frac{\rho_{0i}}{1 + \exp\left(\frac{r - C_i}{0.55}\right)}, \quad (i = n, p)$$
(4)

where

$$\rho_{0n} = \frac{3}{4\pi} \frac{N}{A} \frac{1}{r_{0n}^3}, \quad \rho_{0p} = \frac{3}{4\pi} \frac{Z}{A} \frac{1}{r_{0n}^3}.$$
 (5)

C, the central radius, is given by

$$C = R(1 - \frac{1}{R^2}), \ R = \frac{NR_n + ZR_p}{A}.$$
 (6)

Both neutron and proton sharp radii are assumed as

$$R_n = r_{0n}A^{1/3}, \qquad R_p = r_{0p}A^{1/3},$$
 (7)

and

$$r_{0n} = 1.1375 + 1.875 \times 10^{-4} A,$$
 $r_{0p} = 1.128 \text{ fm.}$ (8)

The Ngô - Ngô density is given as Ngo in our work.

3.1.2 Gupta density distribution 1

The second density distribution is the two parameter Fermi (2pF) density presented by

$$\rho_i(r) = \frac{\rho_{0i}}{1 + \exp\left(\frac{r - R_{0i}}{a_i}\right)}, \quad \rho_{0i} = \frac{3A_i}{4\pi R_{0i}^3} \left(1 + \frac{\pi^2 a_i^2}{R_{0i}^2}\right)^{-1},$$
(9)

where R_{0i} and a_i are half-density radius and surface thickness parameter, respectively. Gupta et al. [18] provided R_{0i} and a_i expressions given by [19]

$$R_{0i} = 0.90106 + 0.10957A_i - 0.0013A_i^2 + 7.71458 \times 10^{-6}A_i^3 - 1.62164 \times 10^{-8}A_i^4, \tag{10}$$

$$a_i = 0.34175 + 0.01234A_i - 2.1864 \times 10^{-4}A_i^2 + 1.46388 \times 10^{-6}A_i^3 - 3.24263 \times 10^{-9}A_i^4. \tag{11}$$

This density is signed as G1 in the present study.



3.1.3 Gupta density distribution 2

Gupta et al. [20] produced different values of R_{0i} and a_i in the following form

$$R_{0i} = 0.9543 + 0.0994A_i - 9.8851 \times 10^{-4}A_i^2 + 4.8399 \times 10^{-6}A_i^3 - 8.4366 \times 10^{-9}A_i^4,$$
(12)

$$a_i = 0.3719 + 0.0086A_i - 1.1898 \times 10^{-4}A_i^2 + 6.1678 \times 10^{-7}A_i^3 - 1.0721 \times 10^{-9}A_i^4$$
 (13)

The other parameters of this density marked as G2 are the same as G1 density.

3.1.4 Wesolowski density distribution

Wesolowski [21] proposed different parameters of Fermi density given by [22]

$$\rho_0 = \frac{3}{4\pi R_0^3} \left(1 + \frac{\pi^2 a^2}{R_0^2} \right)^{-1}, \ a = 0.39 \,\text{fm}, \tag{14}$$

$$R_0 = R' \left[1 - \left(\frac{b}{R'}\right)^2 + \frac{1}{3} \left(\frac{b}{R'}\right)^6 + \dots \right],$$
 (15)

with

$$R' = \left[1.2 - \frac{0.96}{A^{1/3}} \left(\frac{N-Z}{A}\right)\right] A^{1/3}, \ b = \frac{\pi}{\sqrt{3}}a.$$
 (16)

This density is indicated as W.

3.1.5 Schechter density distribution

Schechter et al. [23] provided different values of Fermi parameters as

$$\rho_0 = \frac{0.212}{1 + 2.66A^{-2/3}}, \quad R_0 = 1.04A^{1/3}, \quad a = 0.54 \text{ fm}.$$
(17)

This density is expressed as S.

3.1.6 Moszkowski density distribution

Moszkowski [24] reported 2pF density parameters shown by

$$\rho_0 = 0.16 \text{ nucl./fm}^3$$
, $R_0 = 1.15A^{1/3}$, $a = 0.50 \text{ fm.}$ (18)

Moszkowski density is presented as M.

3.1.7 Harmonic oscillator model density distribution

Another density evaluated in our study is harmonic oscillator density written as

$$\rho(r) = \rho_0(1 + \alpha(\frac{r}{a})^2) \exp(-(\frac{r}{a})^2).$$
 (19)

where α =1.290 and a=1.756 [25]. Harmonic oscillator density is displayed as HO.

3.1.8 Modified harmonic oscillator model density distribution

The last density investigated with this study is modified harmonic oscillator density distribution. This density is the same as the HO density except for α and a free parameters. In this work, α =1.25 and a=1.81 [25]. Modified harmonic oscillator density is displayed as MHO.

3.2 Density distributions of target nuclei

The elastic scattering cross sections of the ¹⁵N nucleus are examined for seven different target nuclei which consist of ⁷Li, ⁹Be, ¹⁰B, ¹¹B, ¹²C, ¹³C, and ²⁷Al.

The density of ⁹Be target is taken as [26]

$$\rho(r) = (A + BC^2r^2)\exp(-C^2r^2) + (D + EF^2r^2)\exp(-F^2r^2),$$
(20)

where A = 0.0651, B = 0.0398, C = 0.5580, D = 0.0544, E = 0.0332, and F = 0.4878.

The ¹³C density is taken as the MHO density in the following form

$$\rho(r) = \rho_0(1 + \xi \frac{r^2}{\alpha^2}) \exp(-\frac{r^2}{\alpha^2}), \tag{21}$$

where ρ_0 , ξ and α are 0.1721884, 1.403 and 1.635, respectively [25].

The densities of 7 Li, 10 B, 11 B, and 12 C targets are produced by

$$\rho(r) = (\xi + \gamma r^2) \exp(-\beta r^2). \tag{22}$$

 ξ , γ and β parameters are shown in Table 1. The density of ²⁷Al target is 2pF density given by

$$\rho(r) = \frac{\rho_0}{1 + \exp(\frac{r-c}{z})}.$$
 (23)

 ρ_0 , c and z values are listed in Table 1.



4 Results and Discussion

The elastic scattering calculations are carried out for eight different densities of ¹⁵N projectile which consist of Ngo, G1, G2, W, S, M, HO, and MHO. The density distributions are displayed as a function of r in Fig. 1. In addition to this, the root mean square (rms) values of these density distributions are given as compared with the literature in Table 2.

The parameters of the imaginary potential are adjusted in order to better reproduce the elastic scattering cross sections of 15 N projectile from different targets. The same potential geometry for all the systems has been used. As a result of preliminary investigations at step intervals of 0.1 and 0.01, r_w and a_w values have been taken as 1.30 fm and 0.50 fm, respectively. Convenient values of W_0 have been determined for constant values of r_w and a_w . While the theoretical calculations are performed, the renormalization (N_R) values have not been changed to determine the compatibility of density distributions with each other. Thus, N_R value has been assumed as unity in all the calculations.

We have obtained the elastic scattering cross sections of $^{15}N + ^7Li$ reaction for eight different densities of ^{15}N nucleus at E_{lab} =81 MeV. We have shown the theoretical results in a comparative form with experimental data in Fig. 2. We have observed that some density distributions have given good results at small angles but not at large angles. Also, we have noticed that the results of some densities such as G1 and G2 are very similar to each other. We have obtained the best results for S and M densities when we have compared the results with each other.

The elastic scattering cross sections of $^{15}N + ^9Be$ reaction at E_{lab} =84 MeV have been calculated by using the double folding model based on the optical model. The results and experimental data have been compared with each other in Fig. 3. It has been seen that the results of the density distributions are very similar to each other at small angles. On the other hand, differences among the results have been observed at large angles. The results are generally consistent with the experimental data except for the Ngo, S and M densities which are incompatible with the small angles of the data.

Another reaction examined in our study is ¹⁵N + ¹⁰B system. The elastic scattering cross sections that acquired for eight different densities of ¹⁵N projectile at incident energy of 43 MeV have been shown together with the experimental data in Fig 4. The theoretical results show a similar behavior with each other at both small and large angles. Additionally, it has been observed that the theoretical results are in good agreement with experimental data especially for Ngo, S and M densities.

The elastic scattering data of 15 N projectile by 11 B target have been obtained by using the double folding model based on the optical model at $E_{\rm lab}$ =43 MeV. Both theoretical results and experimental data have been compared in Fig. 5. While the results of density

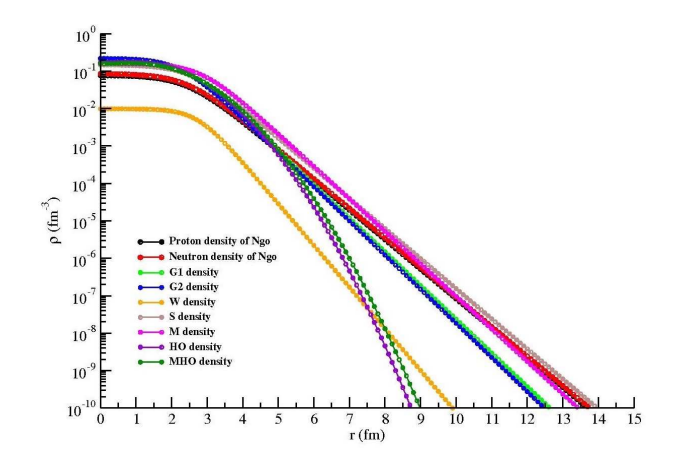


Fig. 1: Ngo, G1, G2, W, S, M, HO and MHO density distributions in logarithmic scale.

distributions show similar behaviors at small angles, differences appear at large angles. On the other hand, it is realized that the results of Ngo and M densities are slightly better than the results of other densities.

The elastic scattering results of 15 N + 12 C reaction which are calculated for eight various density distributions of 15 N nucleus at $E_{\rm lab}$ =81 MeV have been presented together with the experimental data in Fig. 6. The results of G1 density are in good agreement with the data at small angles but not at large angles. The results of S density except for $56^{\circ} < \Theta < 70^{\circ}$ are in very good agreement with the data. Additionally, the results of Ngo and S densities are in very good agreement with the experimental data and are slightly better than the other density results.

The elastic scattering angular distributions of $^{15}N + ^{13}C$ reaction have been analyzed by using the double folding model at E_{lab} =30, 32 and 45 MeV. Both theoretical results and experimental data have been compared in Fig. 7. It has been seen that experimental data have a highly oscillating structure. Therefore, we had a hard time trying to fit the experimental data in the same potential geometry. However, we can say that our results are in harmony with the experimental data. Especially, the results of Ngo and M densities are more compatible with experimental data than other densities.

The last reaction examined in our study is ¹⁵N + ²⁷Al system. The elastic scattering cross sections have been obtained for four different energies such as 32.8, 47.9, 62.0 and 69.8 MeV. It can be seen from Fig. 8 that a good agreement between theoretical results and experimental data has been achieved. Especially, the results of G1, G2, W, and HO densities at 32.8 MeV and the results of G1, G2, W, HO and MHO densities at 47.9 MeV are in very good agreement with the data. The behaviors of all densities at 62.0 and 69.8 MeV are similar to each other and the results are in good agreement with the data.



Table 1: The parameters of Gaussian density for ⁷Li, ¹⁰B, ¹¹B, and ¹²C nuclei, and the parameters of 2pF density for ²⁷Al nucleus.

		2pF							
Nucleus	ξ	γ	β	Ref.	Nucleus	С	z	$ ho_0$	Ref.
⁷ Li	0.1387	0.023204	0.3341	[27]	²⁷ Al	2.84	0.569	0.2015	[30]
$^{10}\mathrm{B}$	0.15924	0.045519	0.341991	[28]					
11 B	0.18465	0.052432	0.350133	[28]					
¹² C	0.1644	0.082003	0.3741	[29]					

Table 2: The rms radii for Ngo, G1, G2, W, S, M, HO, and MHO density distributions in a comparative manner with literature.

Nucleus	Ngo	G1	G2	W	S	M	HO M	ЛНО	Literature
¹⁵ N	2.784	2.515	2.488	2.559	2.824	2.877	2.580	2.655	$2.42 \pm 10^{a}, 2.52^{b}, 2.56 \pm 10^{c}$ $2.58^{d}, 2.65^{e}, 2.58^{f}$

^a From the Glauber model in terms of the optical-limit approximation [31].

Table 3: The cross sections (in mb) obtained for Ngo, G1, G2, W, S, M, HO, and MHO density distributions.

Reaction	Energy (MeV)	Ngo	G1	G2	W	S	M	НО	МНО
$^{15}N + ^{7}Li$	81	1377	1342	1340	1369	1384	1395	1368	1386
$^{15}N + ^{9}Be$	84	1460	1433	1425	1435	1466	1485	1443	1455
$^{15}N + ^{10}B$	43	1255	1186	1177	1189	1263	1274	1198	1217
$^{15}N + ^{11}B$	43	1301	1238	1230	1241	1317	1326	1248	1268
$^{15}N + ^{12}C$	81	1434	1394	1381	1398	1438	1451	1405	1416
	30	1015	963	953	930	1036	1043	944	970
$^{15}N + ^{13}C$	32	1067	980	971	970	1075	1073	988	1013
	45	1265	1199	1182	1196	1274	1291	1210	1225
	32.8	904	824	836	826	917	927	847	868
$^{15}N + ^{27}Al$	47.9	1447	1349	1324	1319	1457	1451	1347	1395
	62.0	1708	1579	1562	1564	1719	1724	1587	1619
	69.8	1820	1597	1603	1608	1820	1828	1655	1696

The cross section is one of important observable parts of nuclear reactions. With this goal, in Table 3, we have given the cross section values of all the reactions and densities analyzed with this work. In addition to this, we have shown the cross sections against E/A_P in Fig. 9. We have observed that the results are in harmony with each other. We have wanted to compare our results with the literature values. But, we could not find the cross sections for these reactions from the literature. As a result of this,

we can say that the cross sections of ¹⁵N projectile with various target nuclei for different densities and energies will be provided to the literature with this study.

4.1 Analytical expressions

It is important to know the potential parameters in the nuclear reactions. Therefore, to obtain simple equations

^b The relativistic mean field (RMF) approach [32].

^c Within the framework of the Glauber model [33].

d,e,f Determined in Ref. [25].



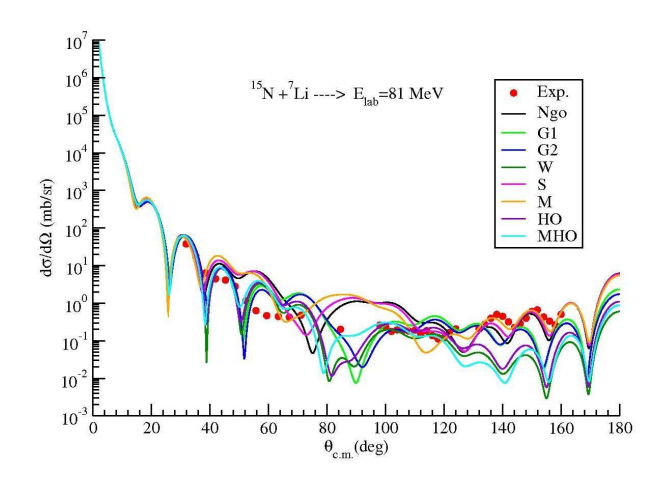


Fig. 2: The elastic scattering cross sections calculated for Ngo, G1, G2, W, S, M, HO and MHO density distributions of the 15 N + 7 Li reaction at E_{Lab} =81 MeV in comparison with the experimental data. The experimental data are taken from Ref. [3].

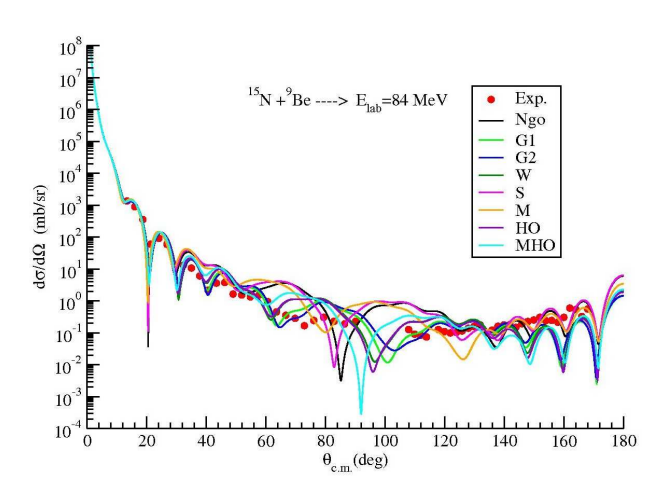


Fig. 3: Same as Fig. 2, but for $^{15}N + ^{9}Be$ reaction at E_{Lab} =84 MeV. The experimental data are taken from Refs. [4]

giving the imaginary potentials will be useful in the analysis of elastic scattering cross sections with the help of folding model calculations. In this context, we achieve imaginary potential equations by using the potential parameters obtained from scattering cross section calculations.

In the present work, we have obtained eight different imaginary potential equations for eight different density distributions investigated with this study. These equations are parameterized in the following forms

Ngo density ---
$$W^{Ngo} = -31.112 + 0.279E + \frac{10.099Z_T}{A_T^{1/3}}$$
(24)

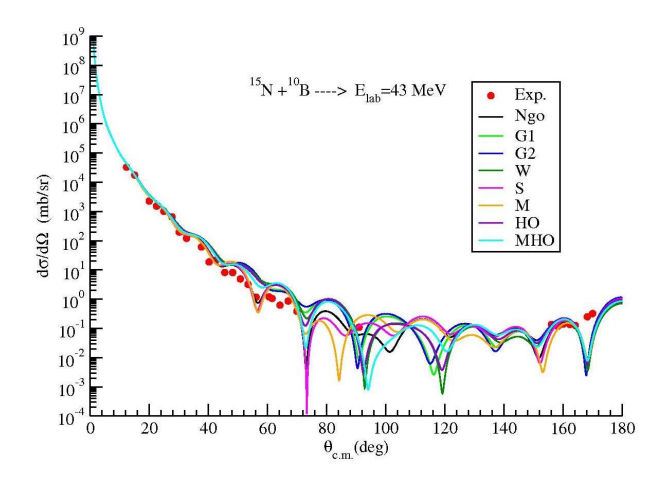


Fig. 4: Same as Fig. 2, but for $^{15}N + ^{10}B$ reaction at E_{Lab} =43 MeV. The experimental data are taken from Ref. [5].

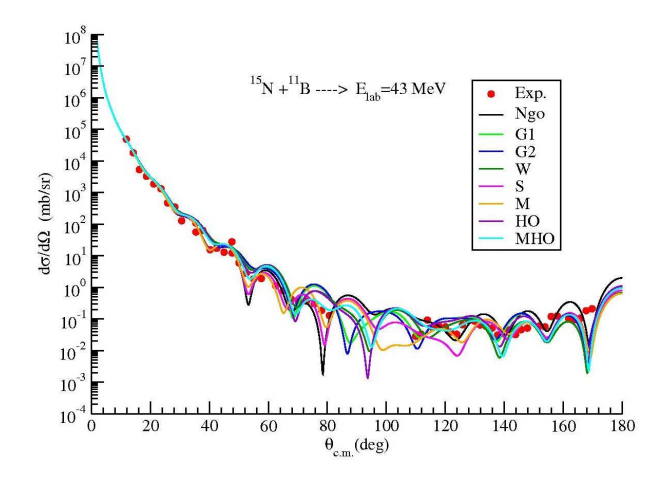


Fig. 5: Same as Fig. 2, but for $^{15}N + ^{11}B$ reaction at E_{Lab} =43 MeV. The experimental data are taken from Ref. [5].

G1 density
$$\longrightarrow W^{G1} = -5.369 + 0.106E + \frac{3.278Z_T}{A_T^{1/3}}$$
(25)

G2 density
$$\longrightarrow W^{G2} = -4.808 + 0.096E + \frac{3.242Z_T}{A_T^{1/3}}$$
(26)

W density
$$\longrightarrow W^W = -5.466 + 0.127E + \frac{2.852Z_T}{A_T^{1/3}}$$
(27)



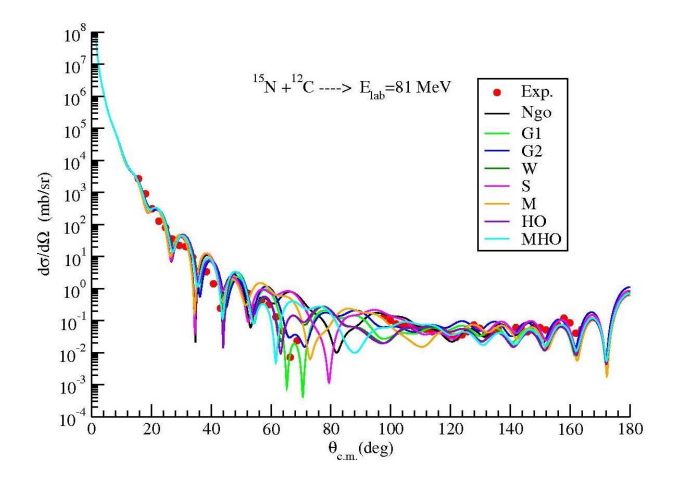


Fig. 6: Same as Fig. 2, but for $^{15}N + ^{12}C$ reaction at E_{Lab} =81 MeV. The experimental data are taken from Ref. [6].

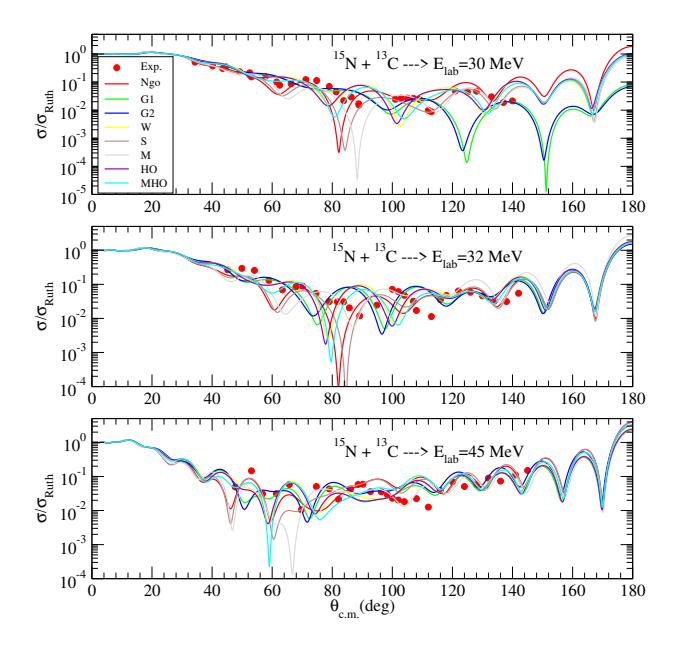
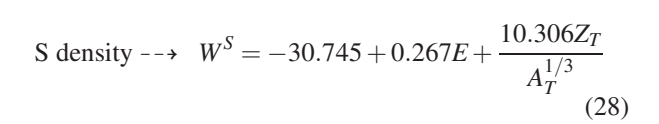


Fig. 7: Same as Fig. 2, but for $^{15}N + ^{13}C$ reaction at E_{Lab} =30, 32, and 45 MeV. The experimental data are taken from Ref. [7].



M density
$$\longrightarrow W^M = -31.420 + 0.279E + \frac{10.388Z_T}{A_T^{1/3}}$$
(29)

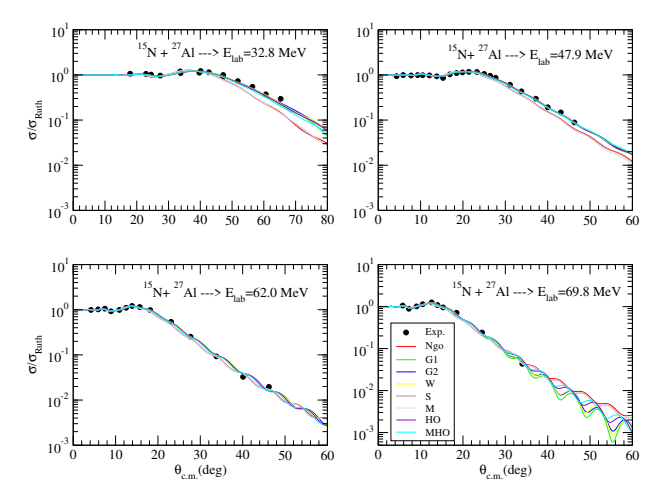


Fig. 8: Same as Fig. 2, but for $^{15}N + ^{27}Al$ reaction at E_{Lab} =32.8, 47.9, 62.0, and 69.8 MeV. The experimental data are taken from Ref. [8].

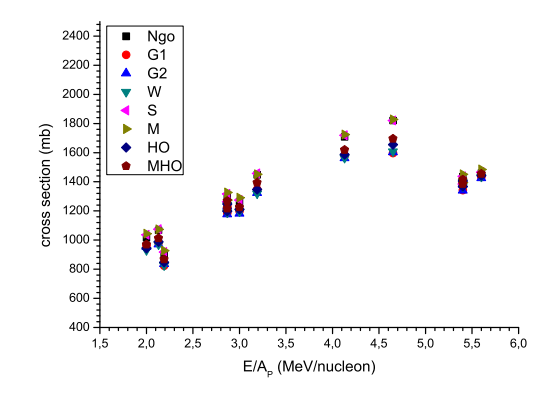


Fig. 9: The cross sections for the calculations with Ngo, G1, G2, W, S, M, HO and MHO density versus E/A_P.

HO density
$$\longrightarrow W^{HO} = -9.817 + 0.147E + \frac{4.213Z_T}{A_T^{1/3}}$$
(30)

MHO density
$$\longrightarrow W^{MHO} = -14.253 + 0.170E + \frac{5.678Z_T}{A_T^{1/3}}$$

where E, Z_T and A_T are the incident energy, atomic and mass numbers of target, respectively.



5 Conclusions

We have analyzed the elastic scattering cross sections of ¹⁵N projectile on ⁷Li, ⁹Be, ¹⁰B, ¹¹B, ¹²C, ¹³C and ²⁷Al target nuclei at different incident energies for eight different densities of ¹⁵N such as Ngo, G1, G2, W, S, M, HO and MHO. In addition to the density distributions known of ¹⁵N nucleus in the literature, we have presented new density distributions with this study. We have obtained the theoretical results describing the elastic scattering experimental data. Also, we have included the cross sections of ¹⁵N projectile with various target nuclei at different densities and energies into the literature. Additionally, we have got new imaginary potential equations for each density distributions examined in the present work. These equations will be useful in the analysis of both elastic scattering cross sections based on the folding model calculations and other nuclear interactions with ¹⁵N nucleus.

References

- [1] https://www.nndc.bnl.gov
- [2] M. Witanowski, Pure Appl. Chem. 37, 225-233 (1974).
- [3] A. T. Rudchik, A. A. Rudchik, L. M. Muravynets, et al., Nucl. Phys. A 958, 234-245 (2017).
- [4] A. T. Rudchik, K. A. Chercas, K. W. Kemper, et al., Nucl. Phys. A 947, 161-172 (2016).
- [5] N. Burtebayev, N. Amangeldi, D. Alimov, et al., Act. Phys. Pol. B 11, 99 (2018).
- [6] A. T. Rudchik, A. A. Rudchik, O. E. Kutsyk, et al., Nucl. Phys. At. Energy 19, 210-219 (2018).
- [7] A. Gamp, P. Braun-Munzinger, C. K. Gelbke, et al., Nucl. Phys. A 250, 341-350 (1975).
- [8] F. W. Prosser, R. A. Racca, K. Danshvar, et al., Phys. Rev. C 21, 1819 (1980).
- [9] M. Aygun, O. Bayrak and Z. Aygun, Quant. Phys. Lett. 6, 149-159 (2017).
- [10] M. Aygun and Z. Aygun, Nucl. Sci. Tech. 28, 86 (2017).
- [11] M. Aygun, Y. Kucuk, I. Boztosun and A. A. Ibraheem, Nucl. Phys. A 848, 245-259 (2010).
- [12] M. Aygun, Eur. Phys. J. A 48, 145 (2012).
- [13] M. Aygun, I. Boztosun, Few-Body Syst. 55, 203-209 (2014)
- [14] G. R. Satchler and W. G. Love, Phys. Rep. 55, 183 (1979).
- [15] I. J. Thompson, Comp. Phys. Rep. 7, 167 (1988).
- [16] C. Ngô, B. Tamain, M. Beiner, et al., Nucl. Phys. A 252, 237 (1975).
- [17] H. Ngô and C. Ngô, Nucl. Phys. A 348, 140 (1980).
- [18] R. K. Gupta, D. Singh and W. Greiner, Phys. Rev. C 75, 024603 (2007).
- [19] O. N. Ghodsi and F. Torabi, Phys. Rev. C 92, 064612 (2015).
- [20] R. K. Gupta, D. Singh, R. Kumar and W. Greiner, J. Phys. G: Nucl. Part. Phys. 36, 075104 (2009).
- [21] E. Wesolowski, J. Phys. G: Nucl. Part. Phys. 11, 1401 (1985).
- [22] N. K. Dhiman, Ukr. J. Phys. 57, 3 (2012).
- [23] H. Schechter and L. F. Canto, Nucl. Phys. A 315, 470 (1979).

- [24] S. A. Moszkowski, Nucl. Phys. A 309, 273 (1978).
- [25] C. W. De Jager, H. De Vries and C. De Vries, At. Data Nucl. Data Tables 14, 479 (1974).
- [26] V. Hnizdo, J. Szymakowski, K. W. Kemper and J. D. Fox, Phys. Rev. C 24, 1495 (1981).
- [27] M. F. Vineyard, J. Cook, K. W. Kemper and M. N. Stephensens, Phys. Rev. C 30, 916 (1984).
- [28] C. W. Glover, K. W. Kemper, L. A. Parks, et al., Nucl. Phys. A 337, 520-532 (1980).
- [29] M. El-Azab Farid and M. A. Hassanain, Nucl. Phys. A 678, 39-75 (2000).
- [30] S. Hossain, M. N. A. Abdullah, Md. Zulfiker Rahman, et al., Phys. Scr. 87, 015201 (2013).
- [31] A. Ozawa, T. Suzuki and I. Tanihata, Nucl. Phys. A 693, 32 (2001).
- [32] J. S. Wang, W. Q. Shen, Z. Y. Zhu, et al., Nucl. Phys. A 691, 618 (2001).
- [33] S. Ahmad, A. A. Usmani and Z. A. Khan, Phys. Rev. C 96, 064602 (2017).